Journal of Power Sources 189 (2009) 571–575

Contents lists available at ScienceDirect

Journal of Power Sources

journal homepage: www.elsevier.com/locate/jpowsour

Short communication

Electrochemical characterization of Li_2MnO_3–$Li[Ni_{1/3}Co_{1/3}Mn_{1/3}]O_2$–$LiNiO_2$ cathode synthesized via co-precipitation for lithium secondary batteries

Jae-Hwan Lim[a], Hyunjoo Bang[a], Ki-Soo Lee[a], K. Amine[b], Yang-Kook Sun[a,*]

[a] Department of Chemical Engineering, Center for Information and Communication Materials, Hanyang University, Seoul 133-791, South Korea
[b] Argonne National Laboratory, Electrochemical Technology Program, Chemical Engineering Division, Argonne, IL 60439, USA

ARTICLE INFO

Article history:
Received 15 August 2008
Received in revised form
23 September 2008
Accepted 1 October 2008
Available online 17 October 2008

Keywords:
Lithium-ion battery
Cathode
Layered material
Li_2MnO_3
Co-precipitation

ABSTRACT

Various compositions of the xLi_2MnO_3–$yLi[Ni_{1/3}Co_{1/3}Mn_{1/3}]O_2$–$zLiNiO_2$ electrode system were synthesized using metal oxide precursor by adopting co-precipitation method. XRD revealed that the prepared cathode materials possess α-$NaFeO_2$ structure with $R\bar{3}m$ space group. Scanning electron micrographs demonstrated the morphology of all the synthesized samples, wherein spherical agglomerates with size of 5–10 μm have been acknowledged. Among the tested samples, $Li[Li_{0.18}Ni_{0.220}Co_{0.120}Mn_{0.480}]O_2$ shows the excellent capacity retention (95.6%) in the voltage range of 2.0–4.6 V and the better rate capability than the other samples. But, on the other hand, $Li[Li_{0.20}Ni_{0.133}Co_{0.133}Mn_{0.534}]O_2$ ($x = 0.6$, $y = 0.4$ and $z = 0.0$) shows the highest discharge capacity. However, the capacity retention of the material at 50 mA g^{-1} is lower than that of $Li[Li_{0.18}Ni_{0.220}Co_{0.120}Mn_{0.480}]O_2$. Furthermore, the capacity retention at 1250 mA g^{-1} is only 42.6% of the capacity obtained at 20 mA g^{-1}.

1. Introduction

In efforts to replace the current $LiCoO_2$ cathode for Li-ion batteries system, many research groups have extensively studied the complex layered compound that has combinational composition of $(x)Li_2MnO_3$ and $(1-x)LiMO_2$, where $LiMO_2$ can be any type of layered materials (e.g., $LiCoO_2$, $LiNi_{0.5}Mn_{0.5}O_2$, $LiNi_{1/3}Mn_{1/3}Co_{1/3}$, etc.), because of its high capacity (>200 mAh g^{-1}) and good structural stability at high charged state (4.5 V) [1–5]. However, these integrated type materials usually experience high irreversible capacity at the first cycle, accompanied with gradual capacity fade during cycling [3–5].

The complexity of these integrated layered system has not been fully understood yet, in terms of the structural features and their electrochemical behaviors. However, extensive research efforts have been given to understand these integrated layered systems because of the demands for new cathode materials to develop next generation of lithium-ion batteries.

In this study, we synthesize various composition of xLi_2MnO_3–$yLi[Ni_{1/3}Co_{1/3}Mn_{1/3}]O_2$–$zLiNiO_2$ system ($0.48 \le x \le 0.60$, $0.32 \le y \le 0.40$ and $0.0 \le z \le 0.2$) via co-precipitation method. The structural and electrochemical properties of prepared material were studied.

2. Experimental

The precursor powders of xLi_2MnO_3–$yLi[Ni_{1/3}Co_{1/3}Mn_{1/3}]O_2$–$zLiNiO_2$ ($0.48 \le x \le 0.60$, $0.32 \le y \le 0.40$ and $0.0 \le z \le 0.2$) were synthesized by co-precipitation method [6]. At the initial stage of the co-precipitation reaction, the irregular shape particles were formed and the formed irregular particles gradually became into spherical particles through vigorous stirring for 12 h in the CSTR (continuous stirred tank reactor). The resulting $[M](OH)_2$ particles were filtered and washed. The obtained spherical particles were dried at 110 °C to remove adsorbed water. A mixture containing stoichiometric amount of $[M](OH)_2$ and an excess amount of $LiOH{\cdot}H_2O$ powder was preheated at 500 °C for 5 h and then finally calcined at 900 °C for 24 h in air.

Powder X-ray diffraction (Rigaku, Rint-2000) using Cu Kα radiation was used to identify crystalline phase of the prepared powders. The morphology of prepared powders was also observed using scanning electron microscopy (SEM, JSM-6340F, JEOL). The chemical compositions of the final powders were determined with an atomic absorption spectroscopy (AAS, Vario 6, Analytic jena).

* Corresponding author. Tel.: +82 2 2220 0524; fax: +82 2 2282 7329.
E-mail address: yksun@hanyang.ac.kr (Y.-K. Sun).

0378-7753/$ – see front matter © 2008 Elsevier B.V. All rights reserved.
doi:10.1016/j.jpowsour.2008.10.035

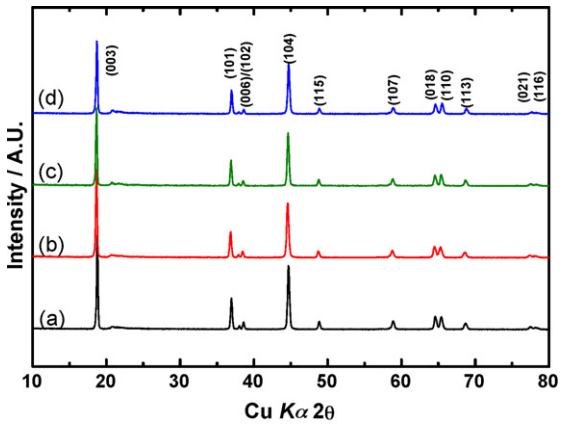

Fig. 1. XRD patterns of the (a) $Li[Li_{0.16}Ni_{0.306}Co_{0.106}Mn_{0.428}]O_2$, (b) $Li[Li_{0.17}Ni_{0.263}Co_{0.113}Mn_{0.454}]O_2$, (c) $Li[Li_{0.18}Ni_{0.220}Co_{0.120}Mn_{0.480}]O_2$, and (d) $Li[Li_{0.20}Ni_{0.133}Co_{0.133}Mn_{0.534}]O_2$.

The electrochemical properties of the prepared powders were evaluated using coin-type cell. The coin cells comprised of the prepared powder as a positive electrode, lithium foil as an anode and an electrolyte having 1 M $LiPF_6$ in a 1:1 vol.% of ethylene carbonate (EC) and diethyl carbonate (DEC) (Cheil Industries Inc., Korea). The micro-porous polypropylene separator was used in these cells. The cell construction was carried out in the Ar-filled dry box. The cells were charged and discharged using charge/discharge battery system (TOSCAT-3000U, Toyo system Co, Japan) in the voltage range of 2.0–4.6 V at a constant current density of 20 mA g^{-1} at 30 °C. Cycle life test was also carried out in the same voltage range of 2.0–4.6 V at 30 °C at the constant current density of 50 mA g^{-1}.

3. Results and discussion

The XRD patterns of xLi_2MnO_3–$yLi[Ni_{1/3}Co_{1/3}Mn_{1/3}]O_2$–$zLiNiO_2$ ($0.48 \le x \le 0.60$, $0.32 \le y \le 0.40$ and $0.0 \le z \le 0.2$) in Fig. 1 show that all the peaks can be indexed based on a hexagonal α-$NaFeO_2$ structure with a space group of $R\bar{3}m$. It can be observed that the weak reflection peak appears between 20° and 25°. The peak is characteristic of complex Li_2MnO_3–$LiMO_2$ phase resulting from the ordering of metal ions (Li, Ni and Mn) and the existence of Li_2MnO_3 phase [7]. Another observation from the XRD patterns is that the peak separation of (1 0 8) and (1 1 0) reflections at 64–66° became clearer as Ni content decreases, indicating that the cation disordering between lithium and metal ions are reduced [8].

The morphology of the metal hydroxide precursors and the lithiated final powders were examined by scanning electron micrography as shown in Fig. 2. It can be observed that the precursors formed spherical agglomerates with the particle size varying from 5 to 10 μm. After calcination of the precursors at 900 °C with $LiOH{\cdot}H_2O$, the primary particle size of the lithiated powders slightly increased, and the morphology and particle size were kept with those of precursor.

Fig. 3 shows the initial charge and discharge voltage profiles of the xLi_2MnO_3–$yLi[Ni_{1/3}Co_{1/3}Mn_{1/3}]O_2$–$zLiNiO_2$ ($0.48 \le x \le 0.60$, $0.32 \le y \le 0.40$ and $0.0 \le z \le 0.2$) cells cycled at a current density of 20 mA g^{-1} between 2.0 and 4.6 V at 30 °C. All the prepared samples have two distinguished voltage regions during the initial charge process. The voltage profiles of all samples start from the initial cell open circuit potential and monotonically increased to 4.45 V with a slope. After voltage reached at around 4.45 V, the voltage plateau was observed. It was reported that the lithium extraction process related to each voltage region originates from the different electrochemical reactions [4,6–8]. The first voltage region below 4.45 V originated from the oxidation of the transitional metal ions to tetravalent ion, while the voltage plateau region locating at 4.45 V is mainly due to electrochemical removal of Li_2O associated with irreversible loss of oxygen from the lattice [1–5,7,8]. It can be observed that the voltage profile of each sample varies with the composition change in particular x value (Li_2MnO_3). As the amount of Li_2MnO_3 (x) increase (consequently, $y+z$ decreases), the charge voltage curve for the first voltage region (below 4.45 V) starts to shift to the higher voltage while the voltage plateau (at 4.45 V) became longer. In addition, the total initial charge capacity and discharge capacity increases as the amount of Li_2MnO_3 increases. The observed discharge capacity for the first cycle is as follows: 203.2, 211.8, 220.9, and 243.8 mAh g^{-1} for $Li[Li_{0.16}Ni_{0.306}Co_{0.106}Mn_{0.428}]O_2$, $Li[Li_{0.17}Ni_{0.263}Co_{0.113}Mn_{0.454}]O_2$, $Li[Li_{0.18}Ni_{0.220}Co_{0.120}Mn_{0.480}]O_2$, and $Li[Li_{0.20}Ni_{0.133}Co_{0.133}Mn_{0.534}]O_2$, respectively.

To understand the contribution of each component of the composite Li_2MnO_3–$Li[Ni_{1/3}Co_{1/3}Mn_{1/3}]O_2$–$LiNiO_2$ material on the charge–discharge behavior, Table 1 summarizes the observed capacity of the each voltage region, corresponding to the electrochemical reaction of each component in the composite electrode. For example, the capacity in the first voltage region (below 4.45 V) is attributed to the oxidation of transitional metal ions in $LiMO_2$ which are $Li[Ni_{1/3}Co_{1/3}Mn_{1/3}]O_2$–$LiNiO_2$ in the tested samples. It can be seen from Table 1 that the initial charge capacity below 4.45 V has a strong relationship with the amount of $LiMO_2$ ($y+z$) in the composite structure. The increase of the initial charge capacity below 4.45 V was observed with the increase in the amount of $y+z$. On the contrary, the value of amount of Li_2MnO_3 (x) influences the initial charge capacity at 4.45 V plateau which is related with lithium extraction in the Li_2MnO_3 [8–10]. The $Li[Li_{0.20}Ni_{0.133}Co_{0.133}Mn_{0.534}]O_2$ with the highest value of Li_2MnO_3 (x) shows the highest charge capacity (195 ± 2 mAh g^{-1}) at 4.45 V plateau at the first cycle.

In order to evaluate the electrochemical properties of the xLi_2MnO_3–$yLi[Ni_{1/3}Co_{1/3}Mn_{1/3}]O_2$–$zLiNiO_2$ ($0.48 \le x \le 0.60$, $0.32 \le y \le 0.40$ and $0.0 \le z \le 0.2$) in high voltage range, the voltage range for charge/discharge changed to 2.0–4.8 V. The applied current density was of 20 mA g^{-1} at 30 °C. Fig. 4 shows the initial charge/discharge voltage profile of the xLi_2MnO_3–$yLi[Ni_{1/3}Co_{1/3}Mn_{1/3}]O_2$–$zLiNiO_2$ ($0.48 \le x \le 0.60$, $0.32 \le y \le 0.40$, $0.0 \le z \le 0.2$) cycled in the high voltage range. The similar voltage profile was observed. The initial charge and discharge capacity for all the samples increases when the higher voltage limit was used.

The cycling performance of the composite xLi_2MnO_3–$yLi[Ni_{1/3}Co_{1/3}Mn_{1/3}]O_2$–$zLiNiO_2$ ($0.48 \le x \le 0.60$, $0.32 \le y \le 0.40$ and $0.0 \le z \le 0.2$) electrodes was compared as shown in Fig. 5. All the tested samples showed a gradual increase of discharge capacity during initial 10 cycles. The cells were cycled between 2.0 and 4.6 V at 50 mA g^{-1}. Among the tested samples, $Li[Li_{0.18}Ni_{0.220}Co_{0.120}Mn_{0.480}]O_2$ and $Li[Li_{0.17}Ni_{0.263}Co_{0.113}Mn_{0.454}]O_2$ shows excellent capacity retention after 100 cycles (95.6% and 94.0%, respectively). Even though $Li[Li_{0.20}Ni_{0.133}Co_{0.133}Mn_{0.534}]O_2$ sample shows the highest discharge capacity, the capacity fade at the tested current density is more rapid than those of $Li[Li_{0.18}Ni_{0.220}Co_{0.120}Mn_{0.480}]O_2$ and $Li[Li_{0.17}Ni_{0.263}Co_{0.113}Mn_{0.454}]O_2$. $Li[Li_{0.16}Ni_{0.306}Co_{0.106}Mn_{0.428}]O_2$ sample revealed most rapid capacity fade (89.7%) in the tested voltage range.

To evaluate the effect of compositional variation of the xLi_2MnO_3–$yLi[Ni_{1/3}Co_{1/3}Mn_{1/3}]O_2$–$zLiNiO_2$ on the rate capability, the cells consisting of each composite electrode were cycled at different current densities and the results are compared in Fig. 6. The

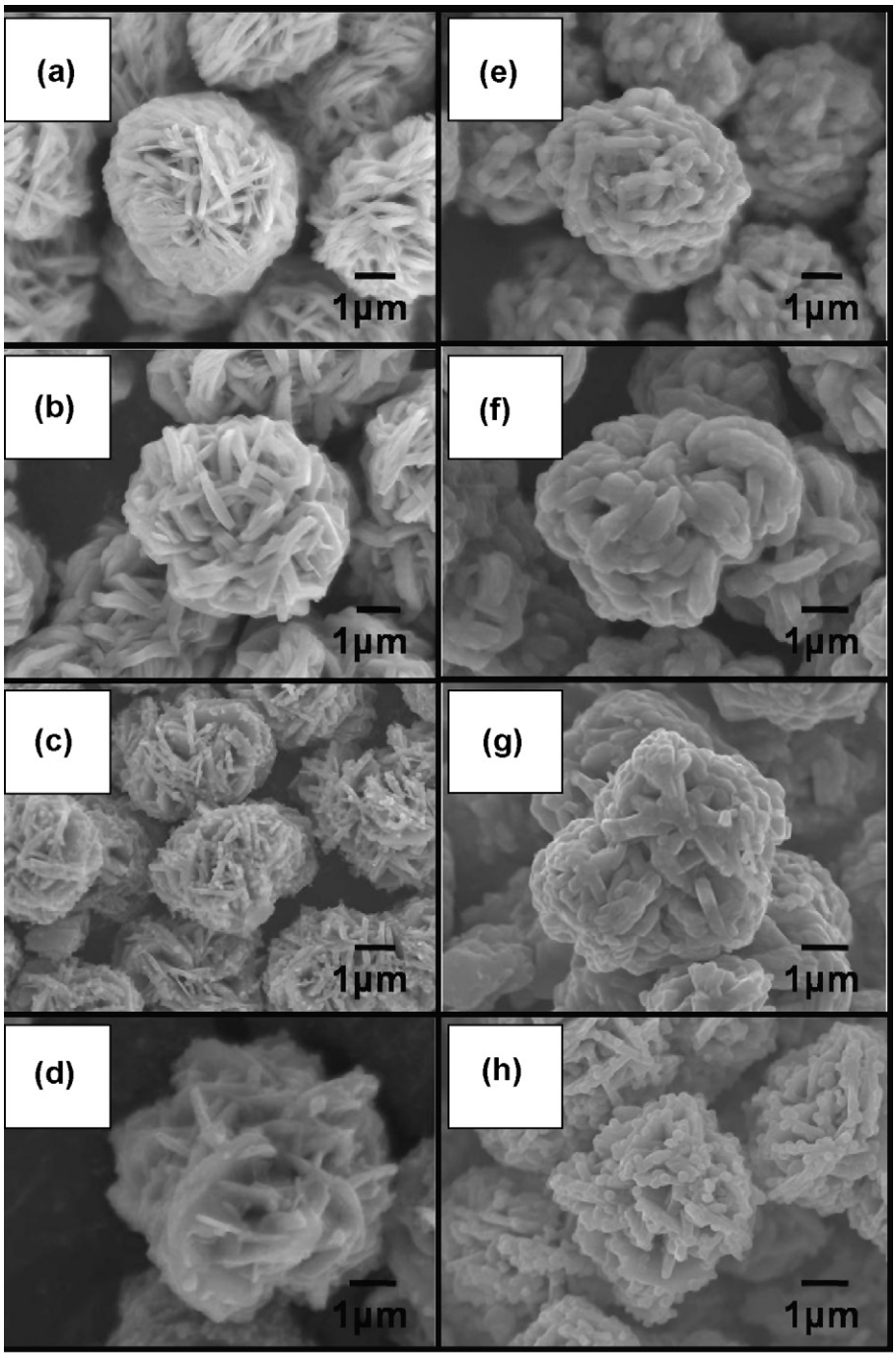

Fig. 2. Scanning electron microscope (SEM) of the precursor ($M(OH)_2$) of the (a) $Ni_{0.365}Co_{0.127}Mn_{0.508}(OH)_2$, (b) $Ni_{0.317}Co_{0.136}Mn_{0.547}(OH)_2$, (c) $Ni_{0.268}Co_{0.146}Mn_{0.586}(OH)_2$, (d) $Ni_{0.166}Co_{0.166}Mn_{0.668}(OH)_2$ and of the final powders of (e) $Li[Li_{0.16}Ni_{0.306}Co_{0.106}Mn_{0.428}]O_2$, (f) $Li[Li_{0.17}Ni_{0.263}Co_{0.113}Mn_{0.454}]O_2$, (g) $Li[Li_{0.18}Ni_{0.220}Co_{0.120}Mn_{0.480}]O_2$, and (h) $Li[Li_{0.20}Ni_{0.133}Co_{0.133}Mn_{0.534}]O_2$.

discharge capacity of all the samples during the initial 3 cycles at the current density of 20 mA g^{-1} keeps increasing and reaches the maximum capacity. As the applied current density increases, all the samples showed gradual decreases of the discharge capacity. Among the tested samples, the $Li[Li_{0.18}Ni_{0.220}Co_{0.120}Mn_{0.480}]O_2$ showed relatively moderate capacity fade as the applied current density increases, which the discharge capacity at 1250 mA g^{-1} still remains 61.6% of the discharge capacity obtained at 20 mA g^{-1} (at 3rd cycle). $Li[Li_{0.20}Ni_{0.133}Co_{0.133}Mn_{0.534}]O_2$ delivered the highest discharge capacity at 20 mA g^{-1}, the discharge capacity at each current density decreases more rapidly than the other samples and showed only 42.6% of the capacity retention at 1250 mA g^{-1}. One of plausible causes for the poor rate capability of $Li[Li_{0.20}Ni_{0.133}Co_{0.133}Mn_{0.534}]$ at high current density may be related to high polarization due to partially blocked Li diffusion pathway. It was reported by Croguennec et al. that the high polarization in $Li[Li_{0.12}Ni_{0.425}Co_{0.15}Mn_{0.425}]O_2$ was usually observed after oxygen loss at the first cycle which caused the movement of Ni into Li layer during oxygen loss and partial blocking of Li diffusion pathway [11]. Since $Li[Li_{0.20}Ni_{0.133}Co_{0.133}Mn_{0.534}]O_2$

Table 1
Chemical composition of the samples and the charge–discharge capacities of composite xLi_2MnO_3–$yLi[Ni_{1/3}Co_{1/3}Mn_{1/3}]O_2$–$zLiNiO_2$ cathode at the first cycle cycled between 2.0 and 4.6 V at 20 mA g^{-1} at 30 °C.

Sample composition[a]	1st charge capacity below 4.45 V (mAh g^{-1})	1st charge capacity at 4.45 V plateau (mAh g^{-1})	Total 1st charge capacity (mAh g^{-1})	1st discharge capacity (mAh g^{-1})	Columbic efficiency (%)	Theoretical capacity[b] (mAh g^{-1})
$Li[Li_{0.16}Ni_{0.306}Co_{0.106}Mn_{0.428}]O_2$ ($x=0.48$, $y=0.32$, $z=0.2$)	162.5	128.4	290.9	203.2	69.6	364
$Li[Li_{0.17}Ni_{0.263}Co_{0.113}Mn_{0.454}]O_2$ ($x=0.51$, $y=0.34$, $z=0.15$)	159.5	147.9	291.2	211.8	72.7	369
$Li[Li_{0.18}Ni_{0.220}Co_{0.120}Mn_{0.480}]O_2$ ($x=0.54$, $y=0.36$, $z=0.1$)	147.9	163.3	311.2	220.9	70.9	375
$Li[Li_{0.20}Ni_{0.133}Co_{0.133}Mn_{0.534}]O_2$ ($x=0.6$, $y=0.4$, $z=0$)	124.2	195.8	320.0	243.8	76.2	386

[a] $x=Li_2MnO_3$, $y=Li[Ni_{1/3}Co_{1/3}Mn_{1/3}]O_2$, and $z=LiNiO_2$.
[b] Theoretical capacity is estimated based on the mass of the electrode material and full utilization lithium content.

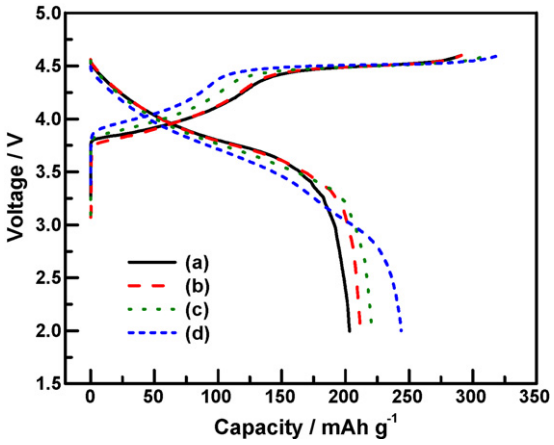

Fig. 3. 1st charge and discharge curves of (a) $Li/Li[Li_{0.16}Ni_{0.306}Co_{0.106}Mn_{0.428}]O_2$ cell, (b) $Li/Li[Li_{0.17}Ni_{0.263}Co_{0.113}Mn_{0.454}]O_2$ cell, (c) $Li/Li[Li_{0.18}Ni_{0.220}Co_{0.120}Mn_{0.480}]O_2$ cell, and (d) $Li/Li[Li_{0.20}Ni_{0.133}Co_{0.133}Mn_{0.534}]O_2$ cell cycled in the voltage range of 2.0–4.6 V at the current density of 20 mA g^{-1}.

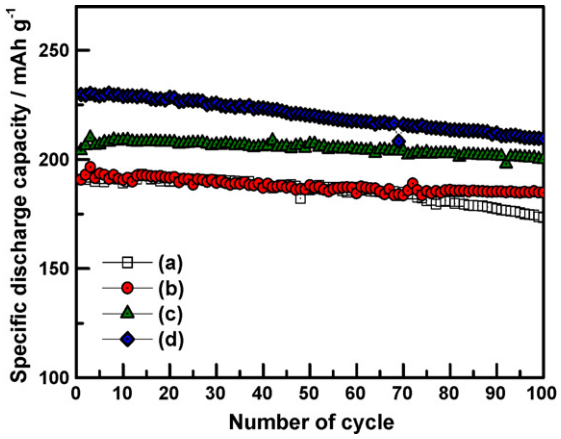

Fig. 5. Comparison of the capacity vs. cycle no of (a) $Li/Li[Li_{0.16}Ni_{0.306}Co_{0.106}Mn_{0.428}]O_2$ cell, (b) $Li/Li[Li_{0.17}Ni_{0.263}Co_{0.113}Mn_{0.454}]O_2$ cell, (c) $Li/Li[Li_{0.18}Ni_{0.220}Co_{0.120}Mn_{0.480}]O_2$ cell, and (d) $Li/Li[Li_{0.20}Ni_{0.133}Co_{0.133}Mn_{0.534}]O_2$ cell in the voltage range of 2.0–4.6 V at the current density of 50 mA g^{-1}.

contains higher amount of Li_2MnO_3 (x) in the structure than the other samples, the relatively large amount of irreversible loss of oxygen could be expected and the poor rate capability of $Li[Li_{0.20}Ni_{0.133}Co_{0.133}Mn_{0.534}]O_2$ would be a consequence [11,12]. Further studies for metal migration, in particular Ni movement into Li layer, and electronic structure change on the compositional variation would provide better way to improve the electrochemical performance of these complex layered compounds.

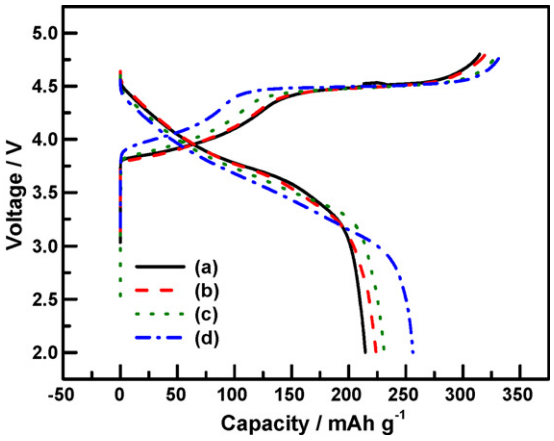

Fig. 4. 1st charge and discharge curves of (a) $Li/Li[Li_{0.16}Ni_{0.306}Co_{0.106}Mn_{0.428}]O_2$ cell, (b) $Li/Li[Li_{0.17}Ni_{0.263}Co_{0.113}Mn_{0.454}]O_2$ cell, (c) $Li/Li[Li_{0.18}Ni_{0.220}Co_{0.120}Mn_{0.480}]O_2$ cell, and (d) $Li/Li[Li_{0.20}Ni_{0.133}Co_{0.133}Mn_{0.534}]O_2$ cell cycled in the high voltage range of 2.0–4.8 V at the current density of 20 mA g^{-1}.

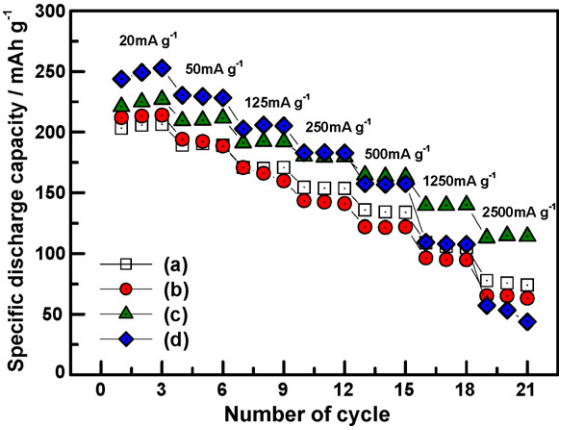

Fig. 6. Comparison of rate capability of (a) $Li/Li[Li_{0.16}Ni_{0.306}Co_{0.106}Mn_{0.428}]O_2$ cell, (b) $Li/Li[Li_{0.17}Ni_{0.263}Co_{0.113}Mn_{0.454}]O_2$ cell, (c) $Li/Li[Li_{0.18}Ni_{0.220}Co_{0.120}Mn_{0.480}]O_2$ cell, and (d) $Li/Li[Li_{0.20}Ni_{0.133}Co_{0.133}Mn_{0.534}]O_2$ cell in the voltage range of 2.0–4.6 V at 30 °C.

4. Conclusions

The composite electrode system of xLi_2MnO_3–$yLi[Ni_{1/3}Co_{1/3}Mn_{1/3}]O_2$–$zLiNiO_2$ powders with various composition ($0.48 \le x \le 0.60$, $0.32 \le y \le 0.40$ and $0.0 \le z \le 0.2$) were synthesized *via* co-precipitation method. The XRD patterns of all the prepared powders show α-$NaFeO_2$ structure with $R\bar{3}m$ space group and the existence of Li_2MnO_3 phase in the composite structure. The morphology of the prepared powders has spherical agglomerates. The initial charge capacity in par-

ticular at 4.45 V increases with an increase of the amount of Li_2MnO_3 (x). On the other hand, an increase of the amount of $y+z$ ($Li[Ni_{1/3}Co_{1/3}Mn_{1/3}]O_2$–$LiNiO_2$) resulted in slight increases of the initial charge capacity below 4.45 V with shift of voltage profile. $Li[Li_{0.18}Ni_{0.220}Co_{0.120}Mn_{0.480}]O_2$ with $x=0.54$ and $y+z=0.46$ shows the excellent capacity retention (95.6%) at 50 mA g^{-1} in the voltage range of 2.0–4.6 V and the better rate capability than the other samples. $Li[Li_{0.20}Ni_{0.133}Co_{0.133}Mn_{0.534}]O_2$ shows the highest initial discharge capacity (243.8 mAh g^{-1}) due to the highest amount of Li_2MnO_3 ($x=0.6$) but reveals the poor capacity retention than that of $Li[Li_{0.18}Ni_{0.220}Co_{0.120}Mn_{0.481}]O_2$. The discharge capacity of $Li[Li_{0.20}Ni_{0.133}Co_{0.133}Mn_{0.534}]O_2$ at the high current density of 1250 mA g^{-1} is only 42.6% of the capacity obtained at 20 mA g^{-1} while $Li[Li_{0.18}Ni_{0.220}Co_{0.120}Mn_{0.480}]O_2$ showed 61.6% capacity retention. The poor rate capability of $Li[Li_{0.20}Ni_{0.133}Co_{0.133}Mn_{0.534}]$ may result from the hindered lithium diffusion caused by the initial large oxygen loss due to the high amount of Li_2MnO_3.

Acknowledgement

This research was supported by Korea Institute of Energy and Resources Technology Evaluation and Planning.

References

[1] C.S. Johnson, J.-S. Kim, C. Lefief, N. Li, J.T. Vaughey, M.M. Thackeray, Electrochem. Commun. 6 (2004) 1085–1091.
[2] Z. Lu, D.D. MacNeil, J.R. Dahn, Electrochem. Solid State Lett. 4 (2001) A191.
[3] S.H. Kang, Y.K. Sun, K. Amine, Electrochem. Solid State Lett. 6 (2003) A183.
[4] A.R. Armstrong, M. Holzapfel, P. Novak, C.S. Johnson, S.H. Kang, M.M. Thackeray, P.G. Bruce, J. Am. Chem. Soc. 128 (2006) 8694.
[5] L. Zhang, H.H. Noguchi, M. Yoshio, J. Power Sources 110 (2002) 57.
[6] M.-H. Lee, Y.-J. Kang, S.-T. Myung, Y.-K. Sun, Electrochim. Acta 50 (2004) 939.
[7] A.R. Armstrong, M. Holzapfel, P. Novák, C.S. Johnson, S.H. Kang, M.M. Thackeray, P.G. Bruce, J. Am. Chem. Soc. 128 (2006) 8694.
[8] T.A. Arunkumar, E. Alvarez, A. Manthiram, J. Electrochem. Soc. 154 (2007) A770.
[9] J. Choi, A. Manthiram, J. Power Sources 162 (2006) 667.
[10] D.-K. Lee, S.-H. Park, K. Amine, H.J. Bang, J. Parakash, Y.-K. Sun, J. Power Sources 162 (2006) 1346.
[11] L. Croguennec, N. Tran, F. Weill, M. Menetrier, C. Delmas, Lithium Battery Discussion-Electrode Materials, Bordeaux-Arcachon, France, May 2005, p. 22 (Abstract T-47).
[12] J. Jiang, J.R. Dahn, Electrochim. Acta 51 (2006) 3413.